Int. J. Electrochem. Sci., 13 **(2018)** 10961 – 10972, doi: 10.20964/2018.11.94

International Journal of
ELECTROCHEMICAL
SCIENCE
www.electrochemsci.org

An Amperometric Sensitive Hydrogen Peroxide Sensor Based on a Silver Nanoparticle-Doped Polyimide-Modified Glassy Carbon Electrode

Lin Chen[1,2], *Yue Wang*[1,*], *Hao Ban*[1], *SiMin Yu*[2], *Dongping Tao*[3], *Zhizhi Hu*[1,*]

[1] School of Chemical Engineering, University of Science and Technology Liaoning, 185 Qianshan Middle Road, High-tech zone, Anshan, LiaoNing, 114051, China.
[2] Department of Chemistry and Materials Engineering, Yingkou Institute of Technology, Yingkou, LiaoNing, 115014, China.
[3] School of Mining Engineering, University of Science and Technology Liaoning, 185 Qianshan Middle Road, High-tech zone, Anshan, LiaoNing, 114051, China.
[*]E-mail: wangyue@ustl.edu.cn, huzhizhi@163.com

Received: 9 July 2018 / *Accepted:* 6 September 2018 / *Published:* 1 October 2018

We report a novel non-enzymatic sensor for the detection of hydrogen peroxide based on a polyimide and silver nanoparticle composite-modified glassy carbon electrode. The structure and morphology of the modified electrode surface were characterized by scanning electron microscopy and atomic force microscopy. The electrochemical performance of the present sensor was evaluated by cyclic voltammetry and amperometry. Under optimal conditions, the calibration plots are linear in the range of 0.01-1 mM, with a detection limit (S/N＝3) of 8.6 μM. The electrode exhibited high stability, great sensitivity, stable reproducibility and fast response times (＜ 5 s). These results show that polyimide can be used as a reliable and long-life sensor for hydrogen peroxide detection, revealing a new application for polyimide.

Keywords: polyimide, silver nanoparticle, hydrogen peroxide, electrochemical determination

1. INTRODUCTION

Hydrogen peroxide (H_2O_2) detection is of great significance not only because of the dramatically increasing demand in medical diagnosis but also because of the pressing requirement in the chemical, food industry, pharmaceutical and environmental fields [1-4]. Various analytical methods and techniques have been developed to monitor H_2O_2, such as chromatography [5], chemiluminescence [6], titrimetry [7] and electrochemistry techniques [8-10]. Numerous enzyme-

based biosensors have been explored for H_2O_2 determination due to their high sensitivity, great selectivity and fast response [11-14]. However, enzyme-based biosensors are inevitably expensive and environmentally sensitive due to the intrinsic nature of enzymes. Compared to enzymatic H_2O_2 biosensors, non-enzymatic H_2O_2 sensors have advantages of lower cost, longer lifetimes and easy preparation and thus have aroused research interest [15-18].

The electrochemical sensing performance can be affected by the morphology, dimension, surface area and composition of materials [19]. Thus, the characteristics and structures of the electro-catalysts are of great importance in the electro-analysis field for improving sensing performance. At present, various nanostructures have been applied for non-enzymatic H_2O_2 detection, including nanoparticles, nanowires, nanosheets and nanoflowers [20-23]. Polyimide (PI) films possess a wonderful combination of performance characteristics, such as excellent mechanical properties, good dimensional stability, good stability and high glass transition temperatures [24]. PI has been applied in the aerospace industry, flexible circuit boards, liquid crystal displays and automobiles as an electric and electronic material [25].

In this paper, we present a novel composite film of silver nanoparticle-doped PI (Ag/PI) on a glassy carbon electrode (GCE) as a catalytic layer for H_2O_2 detection. The fabricated Ag/PI composite exhibits great enzymeless electrocatalytic activity for the determination of H_2O_2. The introduction of silver nanoparticles significantly enhanced the conductivity of PI. Both the stability and long-term lifetime of the present sensor were also improved due to the physical and chemical stability of PI.

2. EXPERIMENTAL

2.1. Materials and reagents

4, 4'-(Hexafluoroisopropylidene)diphthalic anhydride (6FDA) was purchased from ChinaTech (Tianjin) Chemical Co., Ltd., and was recrystallized from acetic anhydride and vacuum dried before use. 2, 2'-Bis(4-hydroxyphenyl)propane (BHPP) was purchased from the Sinosteel Anshan Research Institute of Thermo-Energy Co., Ltd., China. N,N'-Dimethylacetamide (DMAc), 5-fluoro-2-nitrophenol, potassium carbonate, Pd/C (10%), hydrazine hydrate, acetone, nitric acid, anhydrous ethanol, acetic anhydride, pyridine, uric acid (UA), ascorbic acid (AA), dopamine (DA), glucose (glu), fructose (fru), sodium hydroxide (NaOH), phosphoric acid, glacial acetic acid, boric acid and H_2O_2 were obtained from Sinopharm Chemical Reagent Co., Ltd., China. Silver nanoparticles, gold nanoparticles, and copper nanoparticles were purchased from Suzhou Tanfeng Graphene Tech Co., Ltd. To prepare the electrolyte for the acidic, neutral, and alkaline solutions, 0.1 M Britton-Robinson (BR) buffer (prepared by blending 0.1 M NaOH and 0.1 M of a mixture of three types of acid: phosphoric acid, acetic acid, and boric acid) was used. DMAc was dried by anhydrous molecular sieves before use.

2.2. Apparatus

The synthesized monomer and PI were analyzed by ^{1}H-NMR on a Bruker Advance-AV 500

MHz instrument (Germany) in deuterated dimethyl sulfoxide. FT-IR spectra were measured using a Nicolet iS10 (USA) equipped in the range of 500-4000 cm^{-1} with an average scanning frequency of 16 times. The X-ray diffraction (XRD) pattern was acquired from 5º to 60º (*2θ* value) with Cu-Kα radiation (λ=1.541Å) by an X'Pert Powder X-ray diffractometer (PANalytical, Netherlands). The morphologies of PI/GCE and Ag/PI/GCE were observed by field emission scanning electron microscopy (FE-SEM, ΣIGMA-HD, ZEISS, Germany) and atomic force microscopy (AFM, Being Nano-instruments CSPM-5500, BenYuan, China). Electrochemical measurements were performed with a CHI 750D workstation (Shanghai Chenhua, China).

2.3. Monomer synthesis

2.3.1 Synthesis of 2, 2'-bis(3-nitro-4-hydroxyphenyl)propane (BNHPP)

BHPP (6.84 g) was dissolved in acetone (20 mL) in a three-necked flask. Concentrated nitric acid (22 mL) was dropped into the flask with a constant-pressure funnel. The mixture was reacted at 0°C for 6 h to obtain a yellow solid. Finally, the yellow solid was filtered and dried at 100°C (HPLC: 99.7%, yield: 88.5%, melting point: 160.0-162.3 ºC). The detailed reaction procedure is shown in the first step of Fig. S1.

2.3.2 Synthesis of 2, 2'-bis(3-amino-4-hydroxyphenyl)propane(BAHPP)

BNHPP (5.56 g), Pd/C (0.72 g) and ethanol (80 mL) were mixed in a three-necked flask. Hydrazine hydrate (42.8 mL) was then dropped into the mixture within 1 h by a constant-pressure funnel. After reacting at 80 ºC for 24 h, the solution was filtered to remove Pd/C. Finally, the solid was filtered and washed with ethanol to obtain a white compound (BAHPP) after standing a while (HPLC: 98.9%, yield: 89.5%, melting point: 254.9-255.6 ºC). The reaction procedure is shown in the second step of Fig. S1.

2.3.3 Preparation of polyimide (PI)

Briefly, BAHPP (10 mmol) was dissolved in DMAc under nitrogen atmosphere. Subsequently, the reaction mixture was cooled to 0℃ until the solid dissolved entirely. Then, 6FDA (10 mmol) was added immediately to the mixture and stirred for 12 h in a nitrogen atmosphere to obtain a viscous poly(amic acid) solution. Finally, the solution was poured into methanol to obtain a white precipitate, which was collected by filtration and vacuum-dried at 150 ºC for 12 h (Figure S2).

2.3.4 Preparation of the modified electrode

PI (30 mg) was diluted in DMAc solvent (0.57 g) and sonicated for 30 min to prepare a homogeneous solution. The silver nanoparticle suspension was prepared by adding 15 mg of silver

nanoparticles to 0.5 mL of DMAc and sonicating for 30 min. Then, the PI solution was mixed with the silver nanoparticle suspension and sonicated for 30 min to prepare the Ag/PI solution. The glassy carbon electrode (GCE, 3.0 mm in diameter) was mechanically polished successively with 1.0-, 0.3-, and 0.05-μm α-alumina slurries on a micro-cloth to obtain a shiny surface. Finally, the Ag/PI solution was cast onto the GCE surface for 24 h to prepare the sensor.

3. RESULTS AND DISCUSSION

3.1 Structural characterization of polyimide

The structures of BNHPP and BAHPP were confirmed by FT-IR and ^{1}H-NMR. Fig. S3 shows the FT-IR spectra of the dinitro compound (BNHPP, Fig. S3a) and diamine compound (BAHPP, Fig. S3b). The disappearance of the typical absorption peaks of the dinitro group (1530 cm^{-1} and 1350 cm^{-1}) and the appearance of the characteristic absorption peaks of amine groups (3410 cm^{-1} and 3325 cm^{-1}) are good evidence of the successful reduction reaction. Fig. S4 and S5 show the ^{1}H-NMR spectra of BNHPP and BAHPP, respectively. BNHPP: ^{1}H NMR (500 MHz, DMSO-d6) δ 10.86 (s, 2H), 7.74 (d, J = 2.3 Hz, 2H), 7.36 (d, J = 8.9 Hz, 2H), 7.06 (d, J = 8.7 Hz, 2H), 1.63 (s, 6H). BAHPP: ^{1}H NMR (500 MHz, DMSO-d6) δ 8.68 (s, 2H), 6.50 (d, J = 8.0 Hz, 2H), 6.41 (s, 2H), 6.30-6.26 (m, 2H), 4.33 (s, 4H), 1.45 (s, 6H). The result shows that the target product was synthesized successfully.

The FT-IR spectra of polyimide are shown in Fig. S6. The peaks at approximately 1758 cm^{-1}, 1713 cm^{-1}, 1376 cm^{-1} and 720 cm^{-1} correspond to asymmetric and symmetric imide ring stretching vibrations of C=O, C-N vibrations and C=O bending vibrations, respectively. The broad peak around 3400 cm^{-1} corresponds to the asymmetric stretching of the O-H bond [26]. Furthermore, morphological information on the polyimide was obtained by XRD. As shown in Fig. S7, a broad peak was observed in the XRD signals, indicating amorphous character. The intersegmental distance of the polymer was 0.492 nm (2θ=18.01º) due to the presence of hydroxyl groups and six fluoro groups.

3.2 Characterization of PI-modified GCE

Surface morphology is an important factor for adjusting the performance of electrochemical sensors. Fig. 1 shows SEM and AFM images for PI/GCE (A, C) and Ag/PI/GCE (B, D). Fig. 1B indicates full coverage of the silver nanoparticles on the PI substrate. Note that the silver nanoparticles retain their highly stereoscopic structure. In addition, the structure provide a favorable configuration and large electro-catalytic site for the determination of H_2O_2. By comparison with Fig. 1C and 1D, the significantly increased surface height on Ag/PI/GCE is also due to the stereoscopic structure. The large amount of silver nanoparticles adsorbed on the PI composite enhances the electrocatalytic ability for H_2O_2.

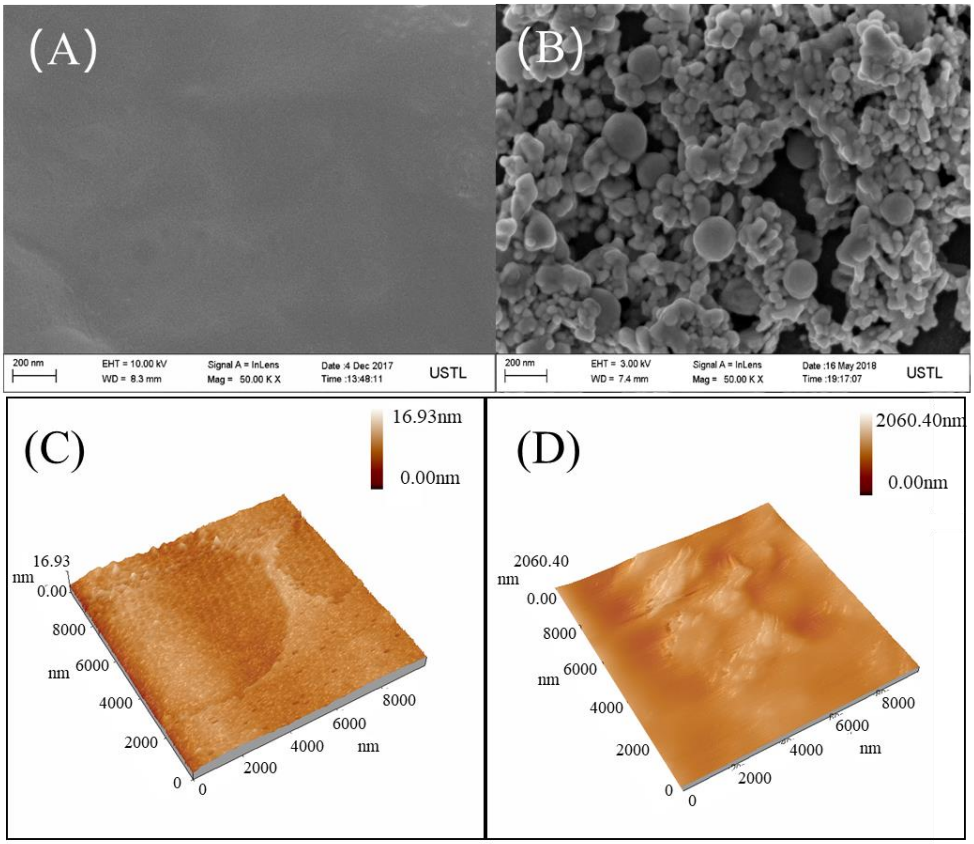

Figure 1. SEM and AFM images of PI/GCE (A, C) and Ag/PI/GCE (B, D).

3.3 Optimization of the experimental variables

The applied potential of the Ag/PI/GCE electrode was first checked based on the current responses with different potentials. As depicted in Fig. 2A, when the potential is in the range of 0 V～-0.3 V, the reductive current response increases with decreasing potential. However, when the potential decreases to more negative regions, the current responses to H_2O_2 decrease because of the severe noise signal and interference from the background current [27]. The working environment is also an important factor for judging the tolerance of sensors. Accordingly, the electrolyte pH was investigated, as shown in Fig. 2B. The best result was obtained at pH 11, but the Ag/PI/GCE sensor shows good responses in a wide range of the pH region. This wide pH range is favorable not only for the commercial applications but also for future study in combination with enzymes. These results show the advantages of this system compared with sensors that can only applied in strong alkaline solution [1, 28]. To further improve the performance of the present sensor, the silver nanoparticle concentration was also investigated. As depicted in Fig. 2C, the concentration of 15 mg/mL gives the best result. We speculate that the optimal amount of silver nanoparticles depends on the capacity of polyimide and the specific stereoscopic structure. Among the three metal nanoparticles, silver shows the best electrocatalytic response toward H_2O_2 (Fig. 3D).

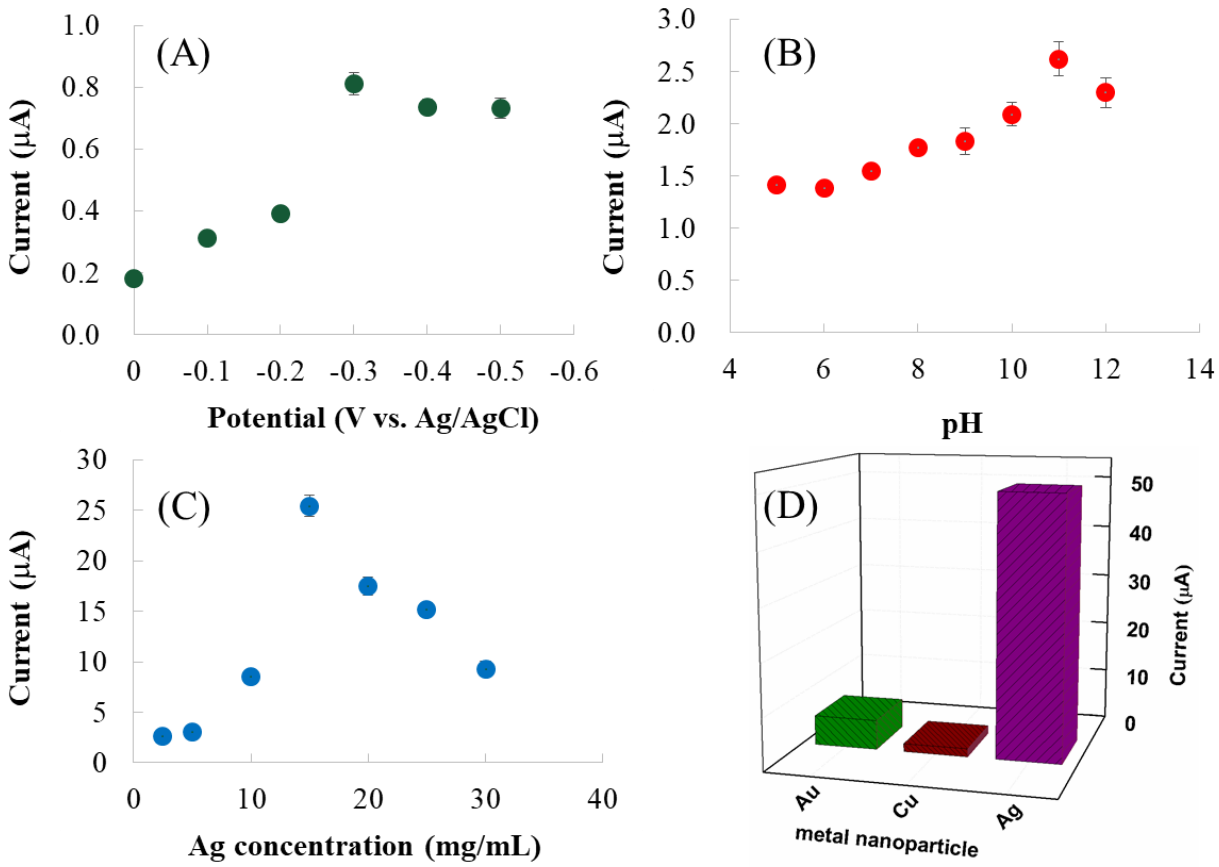

Figure 2. (A) Amperometric responses of Ag/PI/GCE toward 50 μM H_2O_2 in 0.1 M BR (pH 7.0) at various potentials. (B) Amperometric responses of Ag/PI/GCE toward 50 μM H_2O_2 at various electrolyte pH values at -0.3 V. (C) Amperometric responses of Ag/PI/GCE toward 0.5 mM H_2O_2 as a function of the concentration of silver nanoparticles at -0.3 V. (pH 11.0). (D) Effect of different metal nanoparticles on the reduction of 1 mM H_2O_2 at -0.3 V (pH 11.0).

3.4 Electrochemical properties of Ag/PI/GCE

The electrocatalytic performance of Ag/PI/GCE for the determination of H_2O_2 was investigated by cyclic voltammogram (CV) analysis. The reductive current increased with an increasing concentration of H_2O_2, with a good linear range toward H_2O_2 (Fig. 3A). The amperometric reduction current curves obtained for different concentrations of H_2O_2 under the optimized conditions are shown in Figure 4B. The calibration curve for the reduction of H_2O_2 is in the range of 0.01 to 1 mol/L (inset of Fig. 3B), with the regression equation I (μA) ＝5.029 C (μmol/L)-0.0169. The detection limit is 8.6 μM, with an RSD% of 0.9996. Figure 3C is the operation stability with successive addition of 20 μM H_2O_2. The performance was very comparable toward H_2O_2 to that of the amperometric sensor that was reported recently (Table 1) [29-31].

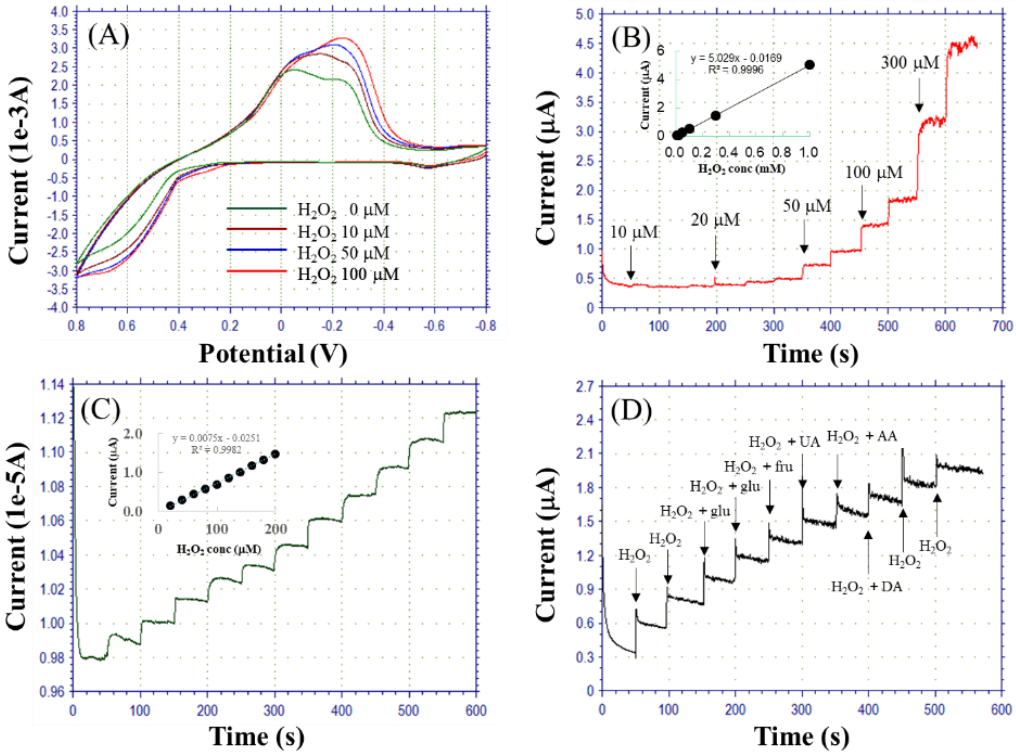

Figure 3. (A) CVs of Ag/PI/GCE at different concentrations of H_2O_2 (0-0.1 mM). (B) Amperometric reductive responses of the Ag/PI/GCE sensor for successive additions of different concentrations of H_2O_2. (The inset is the calibration curve for the concentration range). (C) Amperometric response of 20 μM H_2O_2 on Ag/PI/GCE. (D) Amperometric responses of Ag/PI/GCE for the successive addition of 50 μM H_2O_2 and a mixture of H_2O_2 and 50 μM interferent (The applied potential is -0.3 V vs. Ag/AgCl, pH 11.0 for B-D).

3.5 Selectivity, reproducibility and long-term stability of Ag/PI/GCE

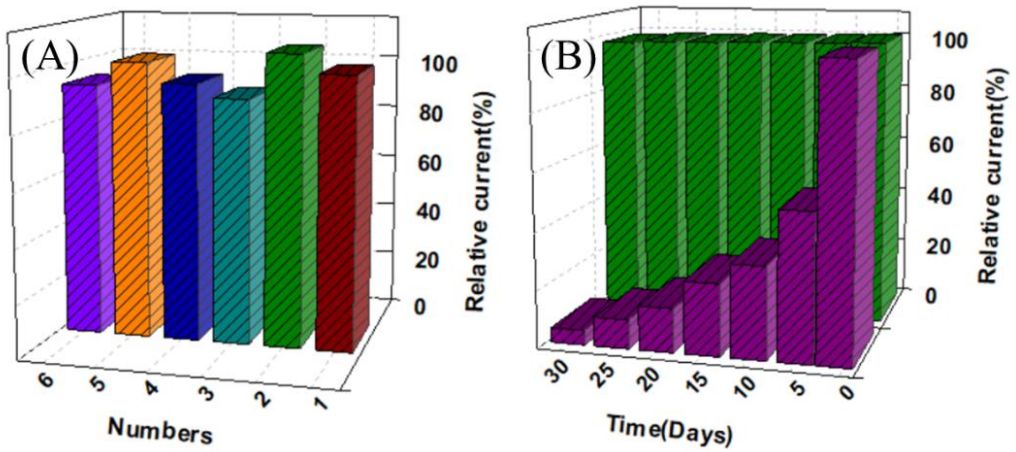

Figure 4. (A) The reproducibility of six independent Ag/PI/GCE sensors for 0.2 mM H_2O_2. (B) Long-term stability of Ag/PI/GCE (green) and Ag/GCE (purple) sensors for 0.2 mM H_2O_2 (Applied potential of -0.3 V vs. Ag/AgCl, 0.1 M BR (pH 11.0)).

Selectivity is an important factor for evaluating sensor performance [32]. Consequently, we investigated the selectivity, as shown in Fig. 3D. As interferents, 50 μM glucose, fructose, UA, DA or AA was mixed with 50 μM H_2O_2. The mixtures were then added to the detection system. Acceptable interference was observed for the Ag/PI/GCE sensor. The current responses due to the interferents are less than 90.5%. Thus, it is safe to assume that the Ag/PI/GCE sensor has good selectivity and anti-interference ability.

To understand the reproducibility of the electrode preparation procedures, six electrodes were prepared under the same conditions. The R.S.D. was 90.3-106.9 % for these electrodes (Fig. 4A). Thus, the preparation process for this sensor has relatively good reproducibility. Lifetime is an important factor for the practical usage of a sensor. The long-term stability of the present sensor toward H_2O_2 sensing was evaluated by detecting H_2O_2 every five days for a month. When not in use, the sensor was stored at room temperature. The Ag/PI/GCE retained approximately 98% of its original activity after 1 month of storage, whereas Ag/GCE lost half of its activity after 5 days of storage (Fig. 4B). These results indicate that the Ag/PI/GCE can maintain excellent function for approximately 1 month. The satisfactory performance is the result of the physical and chemical stability of polyimide.

Table 1. Comparison of the sensors investigated in this study with other H_2O_2 sensors.

Electrode material	Linear range (mmol L^{-1})	LOD (mmol L^{-1})	Ref
CuO/rGO/Cu_2O/Cu	0.5-9.7	0.05	27
Cu_2O/GNs/GCE	0.3-7.8	20.8	29
Chalcopyrite	0.1-30	0.05	17
rGO/CNT/AgNPs/GCE	0.01-10	1.0	30
NiO/α-Fe_2O_3	0.5-3	0.05	31
Ag/PI/GCE	0.01-1	0.0086	This work

Cu_2O, Cu_2O nanocubes; GNs, graphene nanosheets; GCE, glassy carbon electrode; rGO, reduced graphene oxide; CNT, carbon nanotubes; AgNPs, Ag nanoparticles

3.6 Real sample analysis

Practical application is a key step in evaluating sensor performance. To demonstrate the applicability of the Ag/PI/GCE sensor, it was used to detect H_2O_2 in real drinking water. The results obtained both by our method and the standard addition method are shown in Table 2. The results obtained by the sensor were in good agreement with those obtained by the titration method.

Table 2. Ag/PI/GCE sensor applied to drinking water

No.	Measured by proposed H_2O_2 biosensor					$KMnO_4$-titrated method
	Detection (mM)	Added (μM)	Found (μM)	RSD (%)	Recovery (%)	
1	Not found	50.0	52.1	4.9	104.2	51.1

2	Not found	100.0	106.5	4.2	106.5	103.2
3	Not found	200.0	211.0	3.9	105.5	206.0

Dec detection; Rec recovery.

4. CONCLUSION

A polyimide-based sensor was fabricated by one-step physical mixing of silver nanoparticles. The present Ag/PI/GCE exhibited good electrocatalytic activity for the reductive determination of H_2O_2. The sensor has a good linear range from 0.01 to 1 mM, with a detection limit of 8.6 μM. The present sensor combines the advantages of the high stability of polyimide and the high conductivity of Ag nanoparticles. Because of its thermal stability, the sensor can be expected to be applied in extreme environments to broaden its practical usage in the near future.

ACKNOWLEDGMENTS

The authors gratefully acknowledge financial support from the Natural Science Foundation of Liaoning Province (No. 20170540464), the Department of Education of Liaoning (No. 2017LNQN05) and the Foundation of the University of Science and Technology, Liaoning (No. 2016RC12).

References

1. J. Jin, W.Q. Wu, H. Min, H.M. Wu, S.F. Wang, Y. Ding and S.J. Yang, *Microchim. Acta,* 184 (2017) 1389.
2. H.Y. Xia, J.N. Li, L. Ma, Q.F. Liu and J.B. Wang, *J. Alloy. Compd.,* 739 (2018) 764.
3. W. Chen, S. Cai, Q.Q. Ren, W. Wen and Y.D. Zhao, *Analyst,* 137 (2012) 49.
4. L. Zhang, H. Li, Y.H. Ni, J. Li, K.M. Liao and G.C. Zhao, *Electrochem. Commun.,* 11 (2009) 812.
5. U. Pinkernell, S. Effkemann and U. Karst, *Anal. Chem.,* 69 (1997) 3623.
6. D. Achatz, R. Meier, L. Fishcher and O. Wolfbeis, *Angew. Chem. Int. Ed.,* 50 (2011) 260.
7. N.V. Klassen, D. Marchington and H.C.E. McGowan, *Anal. Chem.,* 66 (1994) 2921.
8. F. Wang, W.C. Gong, L.L. Wang and Z.L. Chen, *Microchim. Acta,* 182 (2015) 1949.
9. C.L. Guo, Y.H. Song, H. Wei, P.C. Li, L. Wang, L.L. Sun, Y.J. Sun and Z. Li, *Anal. Bioanal. Chem.,* 389 (2007) 527.
10. E.T.D. Kumar and V. Ganesh, *Appl. Biochem. Biotech.,* 174 (2014) 1043.
11. Y. Wang and Y. Hasebe, *Sensor. Actuat. B-Chem.,* 155 (2011) 722.
12. D. R. Shankaran, N. Uehera and T. Kato, *Anal Bioanal Chem* 374 (2002) 412.
13. J.B. Jia, B.Q. Wang, A.G. Wu, G.J. Cheng, Z. Li, and S.J. Dong, *Anal. Chem.,* 74 (2002) 2217.
14. F. Wang, W.C. Gong, L.L. Wang and Z.L. Chen, *Microchim. Acta,* 182 (2015) 1949.
15. Z.F. Yao, X. Yang, F. Wu, W.L. Wu and F.P. Wu, *Microchim. Acta,* 183 (2016) 2799.
16. S.H. Chen, R. Yuan, Y.Q. Chai and F.X. Hu, *Microchim. Acta,* 180 (2013) 15.
17. Y. Wang, K.J. Zhao, D.P. Tao, F.G. Zhai, H.B. Yang and Z.Q. Zhang, *RSC Adv.,* 8 (2018) 5013.
18. W.Q. Wu, Y.B. Li, J.Y. Jin, H.M. Wu, S.F. Wang and Q.H. Xia, *Sensor Actuat. B-Chem., 232* (2016) 633.
19. S.A. Zaidi and J.H. Shin, *Talanta,* 149 (2016) 30.
20. G.L. Luque, N.F. Ferreyra and G.A. Rivas, *Microchim. Acta,* 152 (2006) 277.
21. F.Y. Xie, X.Q. Cao, F.L. Qu, A.M. Asiri and X.P. Sun, *Sensor. Actuat. B-Chem.,* 255 (2018) 1254.
22. H.Y. Song, C.H. Ma, L.Y. You, Z.Y. Cheng, X.H. Zhang, B.S. Yin, Y.N. Ni and K.Q. Zhang, *Microchim. Acta,* 182 (2015) 1543.
23. S.G. Leonardi, S. Marini, C. Espro, A. Bonavita, S. Galvagno and G. Neri, *Microchim. Acta,* 7

(2017) 2375.
24. G.L. Song, Y. Zhang, D. Wang, C.H. Chen, H.W. Zhou, X.G. Zhao and G.D. Dang, *Polymer,* 54 (2013) 2335.
25. W. Jang, J. Seo, C. Lee, S.H. Peak and H. Han, *J. Appl. Polym. Sci.,* 113 (2009) 976.
26. X.H. Ma, R. Swaidan, Y. Belmabkhout, Y. Zhu, E. Litwiller, M. Jouiad, L. Pinnau and Y. Han, *Macromolecules,* 45 (2012) 3841.
27. C.J. Zhao, X. Wu, P.W. Li, C.H. Zhao and X.Z. Qian, *Microchim. Acta,* 184 (2017) 2341.
28. Z. Zhang, S.Q. Gu, Y.P. Ding, F.F. Zhang and J.D. Jin, *Microchim. Acta,* 180 (2013) 1043.
29. M. M. Liu, R. Liu and W. Chen, *Biosens. Bioelectron.* 45 (2013) 206.
30. Y, Zhang, Z.Y. Wang, Y. Ji, S. Liu and T. Zhang, *RSC Adv.,* 5 (2015) 39037.
31. D.S. achari, C. Santhosh, R. Deivasegamani, R. Nivetha, A. Bhatnagar, S.K. Jeong and A.N. Grace, *Microchim. Acta,* 184 (2017) 3223.
32. Z. Nasri and E. Shams, *Electrochim. Acta,* 54 (2009) 7416.

SUPPLEMENTARY DATA:

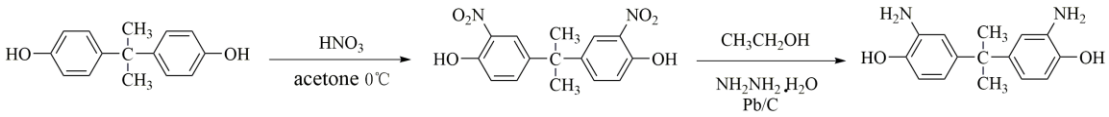

Fig. S1 Synthesis procedures for the dinitro compound (BNHPP) and diamine monomer (BAHPP).

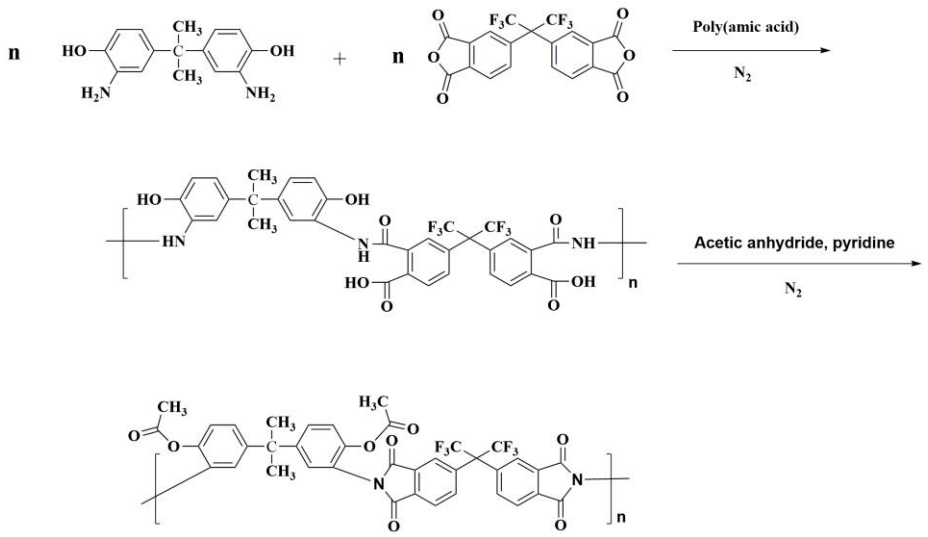

Fig. S2 Synthesis procedures for polyimide

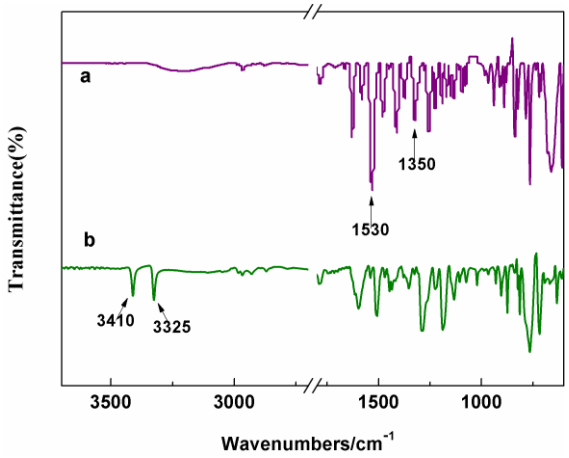

Fig.S3 FT-IR spectra of the dinitro compound (a) and diamine monomer (b)

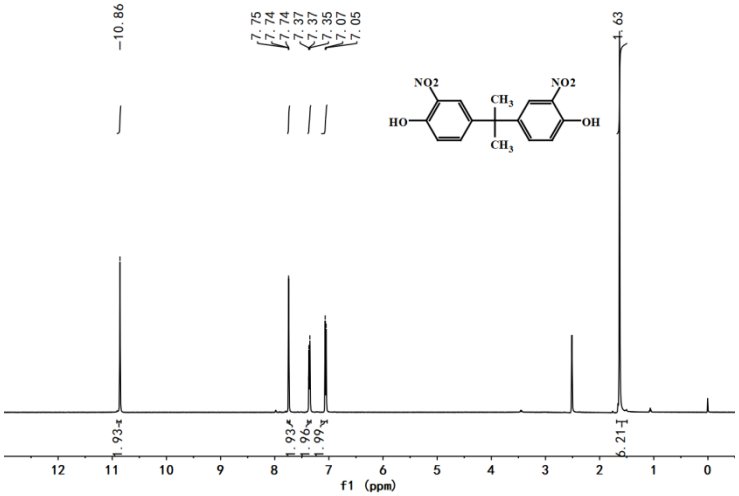

Fig. S4 ^{1}H-NMR spectra of 2, 2'-bis(3-nitro-4-hydroxyphenyl)propane (BNHPP)

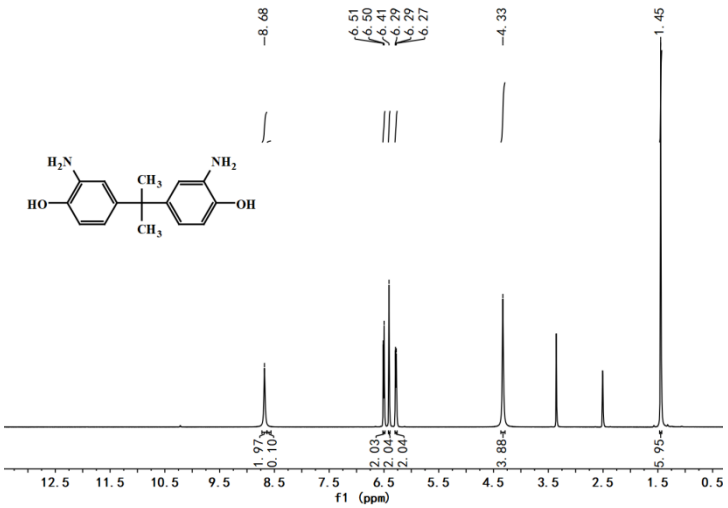

Fig. S5 ^{1}H-NMR spectra of 2, 2'-bis(3-amino-4-hydroxyphenyl)propane (BAHPP)

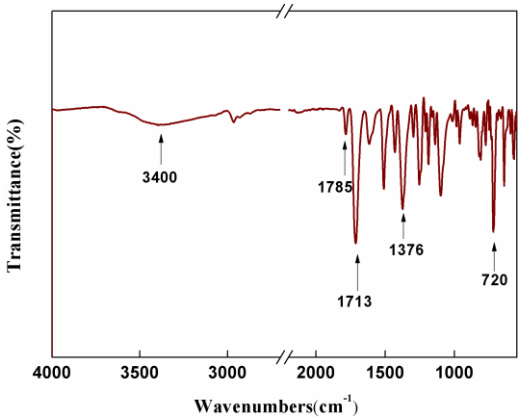

Fig.S6 FT-IR spectrum of polyimide

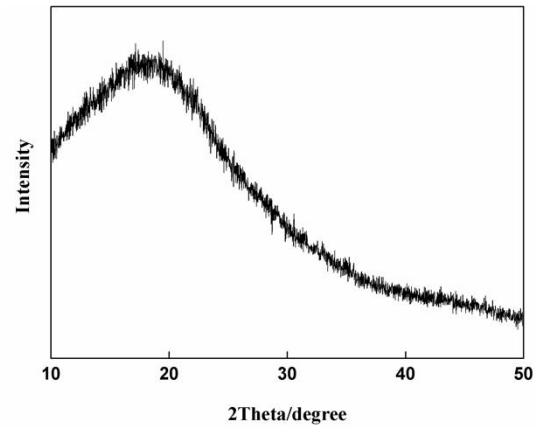

Fig.S7 XRD patterns of polyimide